ACS APPLIED MATERIALS & INTERFACES

Research Article

www.acsami.org

Impact Properties of Thiol–Ene Networks

Olivia D. McNair,[†,‡] Andrew P. Janisse,[†,‡] David E. Krzeminski,[†,‡] Davis E. Brent,[†] Trenton E. Gould,[‡] James W. Rawlins,[†] and Daniel A. Savin*[,†]

[†]School of Polymers and High Performance Materials, University of Southern Mississippi, 118 College Drive #5050, Hattiesburg, Mississippi 39406, United States

[‡]School of Human Performance and Recreation, University of Southern Mississippi, 118 College Drive #5142, Hattiesburg, Mississippi 39406, United States

Supporting Information

ABSTRACT: In this study, a series of thiol–ene networks having glass transition temperatures ranging from −30 to 60 °C were synthesized utilizing several multifunctional thiols and two trifunctional alkenes. Thermomechanical properties were determined using dynamic mechanical analysis, and impact properties were determined using pendulum impact and drop impact testing protocols. The impact behavior was found to directly correlate to the glass transition temperature, except when the temperature at which the impact event occurs overlaps with the range of temperatures corresponding to the viscoelastic dissipation regime of the polymer. Additionally, we discuss insight into the spatial limitations of energy dissipation for thiol–ene network polymers and establish a platform for predictability in similar systems.

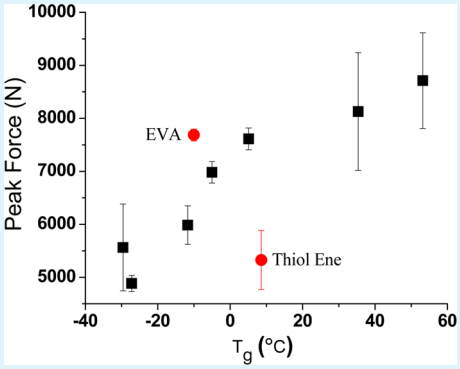

KEYWORDS: *thiol–ene networks, impact, dissipation, thermoset, viscoelasticity, mouthguard*

INTRODUCTION

Polymers are frequently used as energy dissipating materials because of their viscoelastic character and the range of properties attainable by way of adding fillers, manipulating underlying architectures, utilizing copolymers or by simply selecting appropriate monomers.[1−4] Engineers take advantage of the viscoelastic nature of polymers to select damping polymers to absorb energy in the form of noise, vibrations, or mechanical/impact energy, thereby protecting an underlying entity. One area where damping polymers are used extensively is in personal protective equipment (PPE). These materials aim to protect the human body from injuries by absorbing or redirecting kinetic energy from an impact event using a device such as foam padding, hard shells, or even internal devices such as mouthguards.[5] As researchers make advances regarding core mechanisms that facilitate damage, both external and internal, it is increasingly important to develop a new material platform that improves upon the protective capabilities of existing materials.

The damping capabilities of polymers are dictated by a variety of factors, but one important variable is viscoelastic relaxation. Viscoelastic properties of polymers are readily measured using dynamic mechanical analysis (DMA), which affords a great deal of information with respect to temperature and frequency.[6] The loss tangent (tan δ) is the ratio E''/E' of the loss modulus to the storage modulus and reaches a maximum at the glass transition temperature (T_g). This indicates the region of highest mechanical energy dissipation (i.e., loss) for a particular frequency. Viscoelastic damping is then caused by coordinated segmental motions, and for many damping applications a polymer material is selected to have a T_g similar to the use temperature. In general for mouthguard materials, tan δ should exceed 0.3.[7]

Polyethylene-co-vinylacetate (EVA), a semi-crystalline thermoplastic, is utilized in many damping applications for PPE, including mouthguards.[8−10] The T_g of EVA has been reported to be between −30 and −10 °C depending on the method used to measure the value. Based on the fundamentals of damping and viscoelastic relaxation, this material in particular would not demonstrate optimal damping properties at ambient or physiological temperatures as is the case for mouthguards.[7] Processing method and crystallinity are additional mechanisms that reduce energy absorption in EVA. Despite these properties, EVA is commonly used as a material for PPE and mouthguards and will serve as a benchmark for comparison in this investigation.[11,12]

A new class of materials with an established set of improved thermal and physical properties for damping applications is based around thiol–ene networks (TENs). The viscoelastic loss of these amorphous thermoset materials is greater than most polymers in the vicinity of the glass transition.[13] Novel materials based on thiol–ene chemistry have already been suggested as a replacement material for EVA due to their easy fabrication and

Received: August 6, 2013
Accepted: October 14, 2013
Published: October 31, 2013

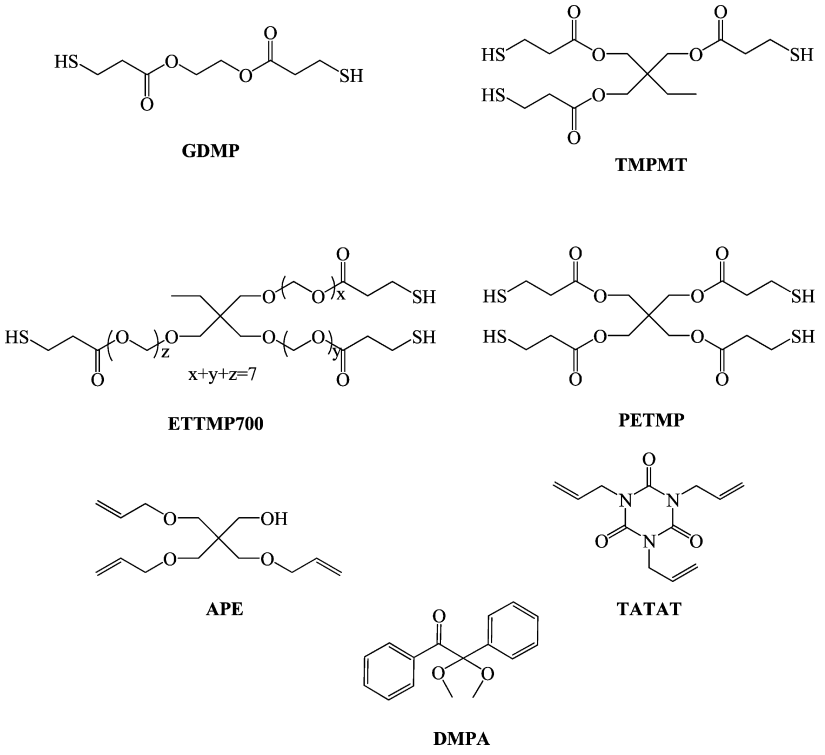

Figure 1. Molecular structures of monomers and photoinitiator (DMPA) used in these studies.

drop-in technology utilizing UV polymerization methods.[14] The radical−step growth reaction mechanism plays a key role in developing highly uniform, low-stress and flexible cross-linked networks.[13,15−17] These aforementioned attributes of TENs make them a rather unique class of materials that could be beneficial for PPE or other applications requiring high damping of mechanical energy.

TENs do offer several advantages over EVA regarding impact energy absorption. First, TENs are typically amorphous (optically clear) materials. The lack of crystalline domains in TENs mean the systems should be inherently static, in contrast to EVA which contains crystalline domains that can grow and order over time.[13] Second, sulfur atoms in thioethers afford more flexibility, similar to ether oxygens in polyether/polyurethane hybrid systems. Thioether flexibility further enhances mobility within the polymers, but the role of mobility in impact energy damping has not been thoroughly investigated for TENs at this point. Finally, a set of TENs with T_g values from sub-zero temperature to temperatures significantly above room temperature are remarkably uniform as demonstrated by their narrow glass transition regions, quantified by the width of tan δ vs. temperature.[13] The lack of network defects such as dangling ends and loops, along with increased flexibility, we anticipate will affect the efficiency of energy dissipation via transfer of viscoelastic relaxation processes. Despite the realized potential of TENs for mechanical energy damping, neither energy dissipation nor energy management by pure TENs has been quantified or analyzed.

Much of the research in TENs has been generally geared towards utilizing chemical methods to control the location of the peak of the tan δ vs. temperature curve in order to achieve optimal glass transition conditions. In 2006, Senyurt and coworkers synthesized a series of TENs of varying T_g values by adding a third acrylate component[14] and found that energy absorption of the resulting networks directly correlated with mole percent acrylate which in turn correlated with T_g. The best performing systems in this study were among those having T_g values proximal to the testing temperature. Other acrylate-based three component TENs have been investigated which also demonstrate that energy absorption is highest when the testing temperature is close to T_g.[18,19] Unfortunately network homogeneity is disrupted when acrylate monomers are used, which is manifested by broad tan δ curves. This is mainly attributed to acrylate rich regions generated by acrylate homopolymerization, which occurs simultaneously with thiol−ene polymerizations. Additionally novel urethane-based TENs have been formulated via multifunctional allyl monomers wherein the glass transition temperatures were controlled via reactive allyl ether diluent.[20] Again, the best energy absorption properties were found when the T_g was proximal to the temperature of the experiment.

Herein we report the synthesis and impact properties of unmodified TENs. A series of TENs were synthesized from commercial monomers using standard UV polymerization techniques. Thermomechanical and viscoelastic properties were determined using DMA, and impact properties and impact energy absorption were measured under ambient conditions via two impact methods. The underlying network architecture was varied by using monomers with two, three or four functional groups while network rigidity was manipulated using a rigid vs. a flexible alkene monomer. Impact behavior was interpreted in terms of polymer viscoelastic properties along with network architecture. The results of this study will connect the anticipated impact behavior of native TENs having a broad range of thermal and mechanical properties, as well as provide a platform for future investigations of modified TENs.

MATERIALS AND METHODS

Materials. A variety of TENs were synthesized from commercially available multifunctional thiol and vinyl monomers. Commercial thiols,

glycol di(3-mercaptopropionate) (GDMP) and ethoxylated trimethylolpropane tri(3-mercaptopropionate) (MW = 708) (ETTMP700) were received from Bruno Bock Thio-Chemicals. Trimethylolpropane tris(3-mercaptopropionate) (TMPT) and pentaerythritol tetra(3-mercaptopropionate) (PETMP) were purchased from Sigma Aldrich Chemical Company. Commercial vinyl monomers, allyl pentaerythritol (APE) and 1,3,5,-triazine-2,4,6 (1H, 3H, 5H)-trione (TATAT) were received from Perstorp and Sigma Aldrich, respectively. Photoinitiator 2, 2- dimethoxy-2-phenylacetophenone (DMPA) was purchased from Sigma Aldrich Chemical Company. All chemicals were used as received without further purification. EVA sheets (Sports Advantage Mouthguard Material, Thermal Forming Soft EVA), thickness = 4 mm, was obtained from Ortho Technology (Tampa, FL). Structures of all monomers and photoinitiator for thiol−ene network formulations are represented in Figure 1.

Synthetic Methods. Thick thermoset plates suitable for impact and thin films for viscoelastic measurements were synthesized via UV polymerization of stoichiometrically balanced monomers mixture containing 0.1 wt % DMPA photoinitiator and a low pressure Hg lamp source. Thin films were synthesized using rectangular Teflon molds (thickness = 0.4 mm) pressed between two glass plates while thicker samples were formed from silicon molds. Thicker samples were initially exposed to a lower intensity light to reduce heat buildup and material warping. The total curing time for all samples was 30 minutes. Following photopolymerization samples were removed from their respective molds and immediately placed in an oven at 90 °C for a period of 1 week to ensure thorough network curing. Samples were equilibrated at room temperature prior to testing.

Real-Time FTIR. Real time kinetics of monomer conversion was collected for each system with a Nicolet 8700 FTIR spectrometer equipped with a KBr beam splitter and MCT/A detector. An external light source, OmicCure Exfo 1000 Series, was guided to the sample via optic cable. Samples were irradiated with UV light (intensity = 25 mW/cm^2) in the range of 320−500 nm while spectra were collected simultaneously at approximately 1 Hz over a range of 650−4000 wavenumbers (cm^{-1}).

Thermomechanical Testing. Dynamic mechanical analysis was performed on films (10 mm × 5 mm × 0.05 mm length × width × thickness) using a Q800 DMA, TA Instruments (New Castle, DE) in tension mode.. Data was collected after first cooling the specimen to −60 °C and annealing for 3 min. Samples were strained at a rate of 1 Hz and to a total 0.05% strain while heating 2°C/min to a final temperature of 100 °C. This same experiment was repeated for ETTMP-TATAT, GDMP-TATAT and TMPT-TATAT at 10 and 100 Hz. T_g was taken as the peak of the tan δ versus temperature curve.

Shore A Hardness, Polymer Density, and M_c Calculation. Shore A hardness of each plate was measured according to ASTM guideline D2240-05.[21] The spring-based device contains an indenter tip (dimensions: tip = 0.031 ± 0.001 mm; taper = 35° ± 0.25°, and shaft = 1.40 ± 0.005 mm), which was smoothly and firmly pressed into each 8 mm thick sample (two layered 4 mm samples). Measurements were taken from three separate regions of material. Polymer density was determined using the Archemedes' method on three samples per formulation as well. Density combined with the E'_{rubber} values from DMA experiments allows calculation of the average molecular weight between cross-links (M_c)

$$M_c = \frac{3\rho RT}{E'}$$

where ρ is the polymer density, R is the gas constant, T is temperature, and E' is the tensile storage modulus at (tan δ_{max} + 40 K).[22]

Impact Testing. Pendulum impact performance was measured via a modified Tinus Olsen (model 892, Horsham, PA, USA). The impact apparatus was adapted by adding a Charpy dart in compliance for a modified ASTM D6110-06f test.[23] The hardened steel dart (taper = 45 ± 2°; radius = 3.17 ± 0.12 mm) was raised to a height corresponding to a standard testing energy of 1.13 J, and the difference in potential energy before and after impact was used to calculate absorbed energy. Impacted samples consisted of two stacked 4 mm thick plates (total sample thickness of 8 mm). Three samples (n = 3) of each TEN formulation and EVA were impacted. The sample order of impacts was not randomized.

Impact performance was also measured via a linear drop test using an instrumented drop tower (Dynatup 9250HV, Instron, Norwood, MA). The drop mass assembly of 5.6 kg contained a piezoelectric 88kN (20 000 lb) load cell tup and a customized 63.5 mm (2.5 in) diameter flat cylindrical steel drop dart to eliminate shear forces during impact.[24] The mass assembly was dropped from a height of 0.08 m resulting in an impact velocity of 1.25 m/sec and a total impact energy of 4.4 J. This energy was consistent with that used by Westerman and coworkers studying EVA, and they cite that this energy is capable of damaging portions of the orofacial complex.[25] Samples were impacted under ambient conditions against a flat, hardened stainless steel anvil and impact velocities were confirmed using an optical velocity flag. Impacted samples were discs of 2 in. diameter and 4 mm thickness. Three discs of each TEN formulation and three cut EVA discs were impacted. The sample order of impacts was not randomized.

Force versus time data were collected via Impulse Data Acquisition software (v. 3.2.30, Instron, Norwood, MA) at 327 kHz. The voltage signal output from the force sensor produced oscillations or "signal ringing" during impact testing and as a result, force data required smoothing. A Savitzky−Golay (SG) filter at 101 points of window under a polynomial order of 2 with no boundary conditions was applied. Selection of a SG filter was utilized because the smoothing function better preserves features of the data such as peak height and width.

RESULTS AND DISCUSSION

Kinetics of Network Formation. Real-time FTIR (RT-FTIR) was used to monitor the kinetics and conversion of thiol and ene moieties in the formation of TENs. Plots for the conversion of thiol and ene as a function of time are given in the Supporting Information (Figure S1) In general, the conversion in terms of thiol consumption was consistent with the conversion in terms of ene consumption. In all cases there was negligible conversion until the sample was illuminated with UV radiation. As these reactions were performed in air, the kinetics of the network formation appear to be insensitive to oxygen. Networks utilizing APE as the ene component showed nearly quantitative conversion after ca. 120 s. For networks using TATAT as the ene component, the conversion after 300 sec is directly correlated with the glass transition temperature of the network (Figure 2) It is expected that higher functionalities and greater monomer rigidity lead to earlier gelation, which decreases collision events and network homogeneity. In addition, as the chains become vitrified, the lack of mobility affects reactivity. The highest conversion with the TATAT ene component was with ETTMP 700, which is the highest molecular weight thiol. The reduced sterics, increased flexibility of this thiol monomer, and lower final T_g allows for a higher collision frequency with the ene monomer. Difunctional GDMP showed a relatively high conversion compared with small, trifunctional and tetrafunctional TMPMT and PETMP, respectively. It is expected that networks from monomers of higher functionality to fail to reach complete conversion because of proximity and mobility of reacting groups at high conversions.[26]

Thermomechanical Properties of TENs Using Dynamic Mechanical Analysis (DMA). One classic characteristic of TENs is the rapid and quantitative kinetics leading to low-stress, uniform, photo-cured materials. The thermomechanical properties of TENs were studied using DMA, and a compilation of the data is given in Table 1.

The glass transition temperature is a very important measurement for damping of polymers. This value is often reported as the temperature associated with maximum loss (a peak in tan δ_{max}). Figure 3 presents tan δ vs. T for each of the

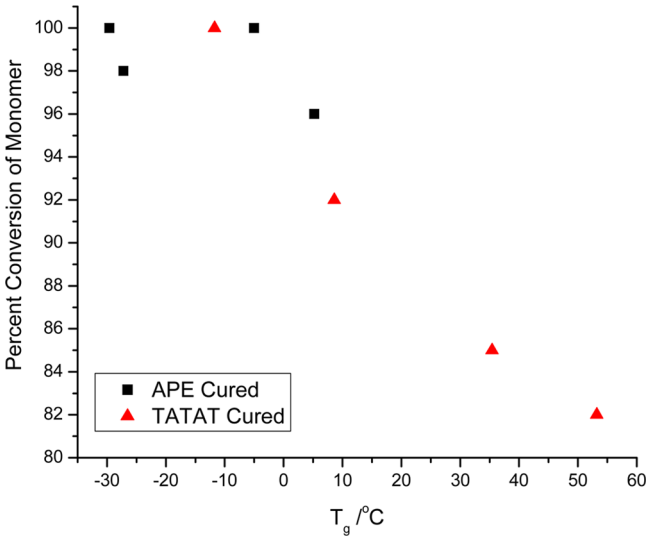

Figure 2. Conversion of monomer as a function of network T_g for TENs synthesized using APE (black squares) and TATAT (red triangles.) The values for T_g were determined using DMA (vide infra). Conversion data were taken from RT-FTIR in Figure S1 in the Supporting Information. In all cases, the thiol and ene conversion were the same except in the case of PETMP-APE. In this case, monomer conversion was taken as the average of thiol and ene conversions.

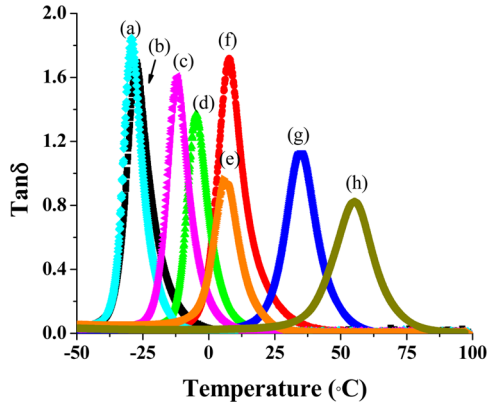

Figure 3. Tan delta versus temperature curves for thiol−ene networks from UV polymerization of the following formulations: (a) ETTMP700-APE, (b) GDMP-APE, (c) ETTMP700-TATAT, (d) TMPT-APE, (e) PETMP-APE, (f) GDMP-TATAT, (g) TMPT-TATAT, and (h) PETMP-TATA.

networks, and the T_g values are indicated in Table 1. Network glass transition temperatures spanned across a broad range of temperatures. This was expected and attributable to the range of monomer functionalities and rigidity that were chosen as part of this investigation. Most T_g values were sub-zero or relatively low, which is typical of TENs because of the flexible thioether linkages throughout the network.[27,28] This effect is more pronounced when the flexible monomer APE was used as the alkene component; using rigid TATAT as the alkene component increased the glass transition temperatures for all thiol formulations (Figure S2 in the Supporting Information)

For a series of TENs, it is expected that the glass transition temperatures will span over a wide range. Microgel formation and vitrification lead to less than quantitative conversion; however TENs are in some ways well-known for their unique network homogeneity and narrow glass transition regions.[13,16,17] Specifically we quantify this parameter using the full width at half-maximum (FWHM) of the transition region, which is the width across at half the peak height of the tan δ versus temperature curve. In this study most systems demonstrated narrow tan δ curves (FWHM < 15 °C) (Table 1). The FWHM values are lowest for systems with low T_g values, which can be attributed to less complex curing mechanics from low viscosity and low functionality monomers.[14,18,20] A slightly broader FWHM is observed for the transition region of those networks with T_g values greater than room temperature such as TMPT-TATAT and PETMP-TATAT.

Tan δ vs. temperature curves of most systems were narrow and possessed relatively high peak values. Since the tan δ is the ratio of E'' to E', systems with high tan δ would demonstrate high energy dissipation at the temperature associated with the peak values. The peak tan δ values and temperatures associated with maximum loss are shown in Figure 3. This significance here is that we demonstrate the capacity to design TEN systems that will absorb mechanical energy at a specific temperature based simply on monomer choice. Our group had previously demonstrated this capability utilizing a third thiol component.[29] Given the typically poor mechanical properties of TENs in terms of tensile properties, it is understandable why a third component may be necessary, but until now a platform for a base system performance was never available.[19,20,30]

Figure 4 shows isochronal plots of the storage modulus E' as a function of temperature. The TENs demonstrated typical behaviors such that at low temperatures E' values were high and as the polymers passed through the glass transition region, E' decreased approximately 2.5 decades before reaching the rubber plateau regime at higher temperatures. Comparing systems synthesized with the same thiol monomer but different ene

Table 1. Compilation of DMA Results for TENs[a]

sample	T_g (°C)	FWHM (°C)	E'_{rubber} (MPA)	density (g/mL)	M_c (g/mol)
GDMP-APE	−27.2 ± 0.6	10.3 ± 0.1	5.8 ± 0.2	1.22 ± 0.01	1470
GDMP-TATAT	8.6 ± 0.9	10.9 ± 0.6	5.9 ± 1	1.31 ± 0.01	1780
TMPT-APE	−5.0 ± 0.4	8.9 ± 0.6	15 ± 2	1.21 ± 0.01	630
TMPT-TATAT	35.4 ± 0.4	13.2 ± 0.2	15 ± 2	1.29 ± 0.03	740
ETTMP700-APE	−29.6 ± 0.3	9.2 ± 0.5	7.5 ± 2	1.19 ± 0.01	1120
ETTMP700-TATAT	−11.7 ± 0.4	10.0 ± 0.5	8.8 ± 0.8	1.25 ± 0.01	1070
PETMP-APE	5.1 ± 0.5	11.6 ± 0.4	17.7 ± 2	1.25 ± 0.01	560
PETMP-TATAT	53.2 ± 2	17.5 ± 0.2	19.8 ± 0.8	1.30 ± 0.03	600
EVA	−10 ± 2	39 ± 1			

[a] T_g was determined from $(\tan \delta)_{max}$, E'_{rubber} is the storage modulus at T_g + 40 K, FWHM is the full width at half maximum of tan δ vs. T, and density was measured using Archmedes' method.

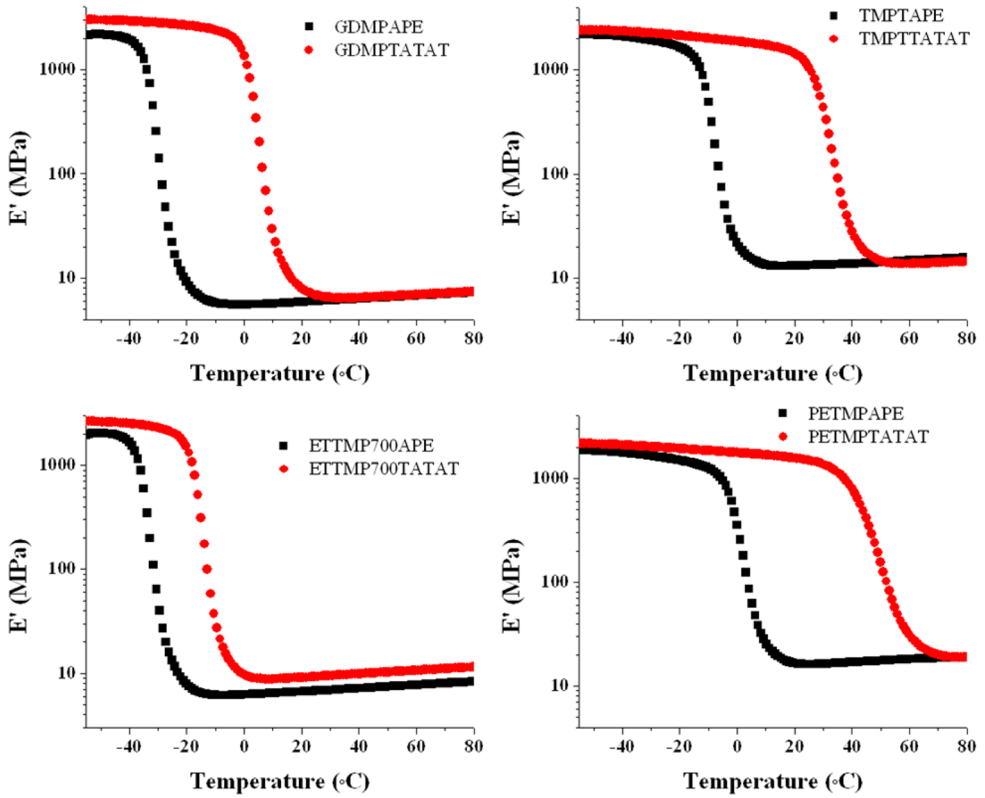

Figure 4. Storage modulus versus temperature for thiol−ene networks cured via UV polymerization with 1 wt % DMPA photoinitiator. DMA was conducted from −60 °C to 120 °C at 2 °C/min to 0.05% strain at a frequency of 1 Hz. Plots are only shown to 80 °C to allow direct comparison.

Table 2. Compilation of Impact Results for TENs

		linear drop testing			
sample	pendulum energy Abs (% of 1.13 J)	peak force (N)	time to peak (ms)	Shore A hardness	tan δ > 0.3 (°C range)
GDMP-APE	shattered	4900 ± 150	1.64 ± 0.06	24 ± 4	−34 to −14
GDMP-TATAT	89	5300 ± 560	1.04 ± 0.4	51 ± 3	0 to 22
TMPT-APE	49	7000 ± 200	0.86 ± 0.07	76 ± 2	−12 to 5
TMPT-TATAT	49	8100 ± 1100	0.80 ± 0.02	>100	26 to 47
ETTMP700-APE	shattered	5600 ± 800	1.46 ± 0.1	28 ± 2	−36 to −18
ETTMP700-TATAT	40	6000 ± 360	1.21 ± 0.2	41 ± 4	−19 to −1
PETMP-APE	74	7600 ± 200	0.62 ± 0.06	81 ± 4	−3 to 14
PETMP-TATAT	shattered	8700 ± 900	0.60 ± 0.06	84 ± 1	42 to 64
EVA	60	7700 ± 110	0.75 ± 0.01	83 ± 1	

monomers, the glassy moduli were higher for systems containing the TATAT monomer which suggests higher packing efficiency within these polymer networks. The most likely reason for this is that the more rigid TATAT monomer is relatively flat and potentially packs better. This behavior is consistent with measured differences in density of the networks (Table 1.)

The storage modulus in the rubbery regime is directly related to M_c for thermosets, such that higher modulus translates to lower M_c or higher cross-link densities. In this study we purposely selected alkene monomers with similar functionality and molecular weight to directly compare systems having different levels of rigidity but similar cross-link densities. In Figure 4, the storage moduli converge for temperatures above T_g, with the exception of ETTMP700, suggesting a similar crosslink density. M_c values were calculated using the polymer density, and the E' taken at $T = T_g + 40$ K.[22] Within experimental error, M_c values directly correlate with monomer molecular weights. The slight differences between groups may be attributed to packing differences between TATAT and APE monomers, or differences in monomer conversion. Additionally APE contains a pendent hydroxyl group which can promote hydrogen bonding with surrounding hydroxyl groups, especially for lower T_g networks.

Impact Properties of TENs. To fully realize the energy-absorbing capacity of TENs for use in mouthguards and other PPE, it is necessary to gain quantitative information regarding transmitted forces, as well as energy absorbed, during the impact event. We present here results from two different impact experiments: (1) pendulum impact, which indicates the total energy absorbed, and (2) linear drop impact testing, which allows us to measure the forces generated during the impact event, and specifically the trace of those forces throughout the duration of the impact. Our benchmark material is EVA, which is used in common commercial mouthguards. Impact results are compiled in Table 2 and will be discussed below.

Pendulum Impact Properties of TENs. The pendulum impact test has been used in previous investigations to measure

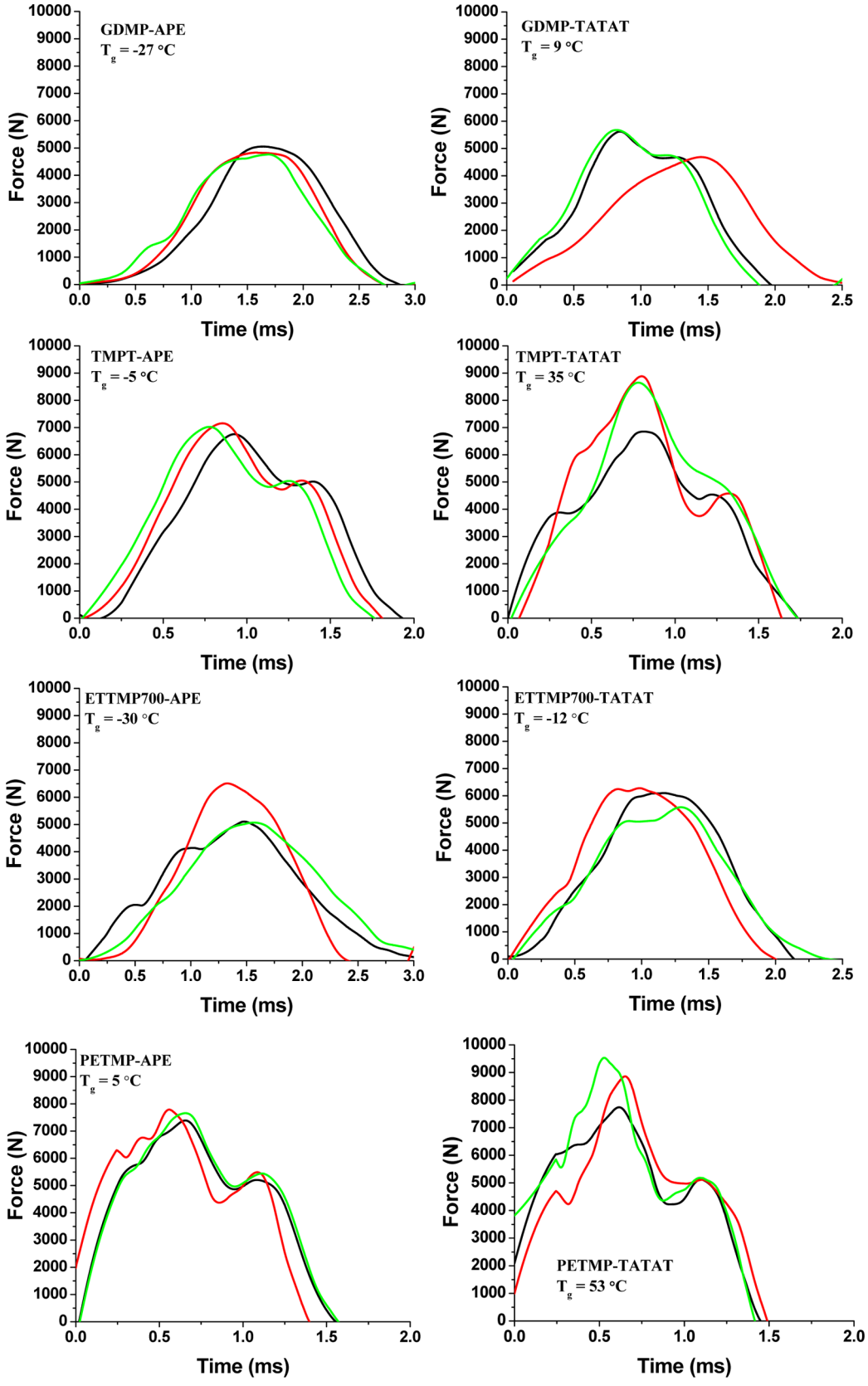

Figure 5. Smoothed force versus time curves for UV-polymerized TENs.

percent of energy absorption for thiol−ene networks modified with acrylates and urethanes, but not unmodified TENs.[7] During this investigation, many samples failed (shattered) from this type of impact event, specifically those containing APE monomer. The lower T_g values, combined with lower packing efficiency, was insufficient for the more concentrated energies of the pendulum impact event; the tup is rounded and contacts a relatively small surface area, theoretically leading to high localized pressures.

Three of the thiol−ene samples studied absorb between 40 and 50% of energy from a 1.13 J pendulum impact event. Systems which demonstrated this type of behavior had subzero T_g values, which in turn means that under ambient conditions such as room temperature, polymer networks are rubbery and elastic, i.e, above the temperature range of effective viscoelastic dissipation where tan $\delta > 0.3$. Two systems that demonstrated the best pendulum impact properties were GDMP-TATAT and PETME-APE, which absorbed 89 and 74% of 1.13 J impact, respectively. Both of these systems had higher impact energy absorption compared with EVA, which under similar test conditions absorbs about 60% of the impact energy.[7] This behavior was expected for GDMP-TATAT because the testing temperature overlaps with the temperature range where tan $\delta > 0.3$ (Table 2). The behavior of PETMP-APE was not so obvious; one way to explain the observed behavior is to consider that some viscoelastic dissipation is possible under the testing conditions of this experiment. For example, there is still a small amount of overlap with the tail of the tan δ vs. temperature curve. In addition, the impact energy absorption is lower for PETMP-APE compared with GDMP-TATAT, and correlates directly with tan δ at the testing temperature.

Although the pendulum impact test allows us to compare these systems with others in the literature, it is a mere snapshot of an impact event. A more detailed analysis is realized using a linear drop testing system. This allows us to measure the forces generated during the impact event, to trace of those forces throughout the duration of the impact, and to interpret in terms of how the material manages the energy from an impact event. Because there are often dimensional limitations on damping materials, we used 4 mm thick slabs of TEN material and 4.4 J of impact energy; this is the most appropriate thickness for a mouthguard,[8] and this energy was previously used to test impact properties of 4 mm thick EVA.[25] Transmitted force loads were plotted against time, constructing impulse curves for an EVA benchmark material (Figure S3 in the Supporting Information) and TENs (Figure 5) The three curves shown are three independent experiments to demonstrate consistency. In this experiment, we are interested in the peak force, the time to peak force, and the shape of the impulse curve. The values measured for EVA were in line with previously published data.[7]

Energy Management of Thiol−Ene Networks: Glassy, Rubbery, and Intermediate Systems. The time dependence and load management of an impact event is important for any damping material. Ideally, an impact will span over a longer period of time, the peak force values will be lower, and the material will absorb more energy. Figure 5 shows impulse curves for 4 mm thick TEN thermosets.

The impulse curves of the TENs demonstrated clear trends in terms of time to peak force and total impact time. Systems having subzero glass transition temperatures, GDMP-APE, ETTMP700-APE, and ETTMP700-TATAT, demonstrate the highest mean times to peak force values: 1.64, 1.46, and 1.15 ms, respectively. This is likely due to compliance and deformation of the material under compression, which is supported by the lowest Shore A hardness values for these networks (Table 2.) In addition, the impulse curves generally had a traditional bell-shape or a plateau, with low peak force values in comparison. These materials deform and dissipate energy effectively because their T_g values are so far (ca. 50 °C) below ambient temperature. The impulse curves of TENs with T_g values above room temperature, i.e., TMPT-TATAT and PETMP-TATAT, both showed very low time to peak force and high Shore A hardness; these systems had time to peak force values approximately one millisecond or less. The correlation between time to peak force and glass transition temperature is not unexpected. Higher T_g systems would be more glassy at ambient temperature and display less deformation upon an impact event, whereas lower T_g systems would respond more elastically. The elastic nature of the rubbery systems would translate to an extension of the time response under compression, or higher strains during an impact event. The peak forces trend inversely with time to peak force, whereby lower peak forces correlated to longer times and vice versa. Materials with high T_g values are unable to deform under test conditions and do not dissipate energy as effectively. As such, the impulse curves are noisy and show sharp peaks as a function of time. GDMP-TATAT, TMPT-APE and PETMP-APE networks exhibited T_g values in the vicinity of the impact testing temperature. These impulse curves generally had a longer time to peak force, and exhibited an apparent yielding (plateau after peak force) at longer times.

To compare characteristic impulse properties of TENs to a commercial damping material, we measured the impulse properties of EVA (see Figure S3 in the Supporting Information). The average peak force value of EVA was 7700 N which was similar to literature values reported for the same energy (4.4 J) and similar impact surface.[25] TENs with T_g values comparable to EVA have lower peak forces (i.e., 5600 N and 7000 N for ETTMP700-TATAT and TMPT-APE, respectively.) The time to peak force for EVA was 0.75 seconds on average, which was faster than any of the TENs having a subzero glass transition temperatures. The semicrystalline morphology of EVA is most likely responsible for the shorter time response and higher peak force values. In fact, the Shore A hardness values of EVA are more comparable to TENs with higher T_g values such as PETMP-APE or PETMP-TATAT. Therefore even though the T_g of EVA is below zero, the crystalline domains effectively harden the material, which proves to have an adverse effect on impact behavior and stress management for EVA. The lack of crystalline domains and the cross-linked nature of TENs give them a significant advantage over thermoplastic EVA and these appear to be ideal systems for future investigations for damping polymers.

Dependence of Peak Force on T_g. Figure 6 shows the peak force (at ambient temperature) as a function of T_g for all thiol−ene systems studied, as well as our EVA benchmark. Peak force of the TEN materials showed a nearly linear relationship with T_g such that systems with low T_g values demonstrated low peak

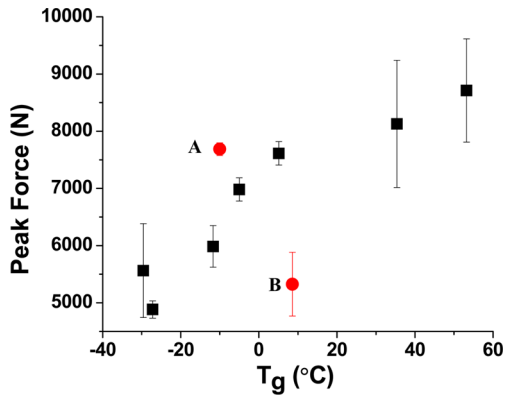

Figure 6. Peak force versus T_g for TENs. Point A is representative of an EVA mouthguard material and point B is GDMP-TATAT.

force values and those with high T_g values had higher peak forces. One-way ANOVA indicated a statistical difference ($F = 14.6$, $p < .001$) in peak force between the materials.

It stands to reason that the location of the glass transition temperature relative to the test temperature would indeed affect impact performance because of the large span of temperature dependent relaxations in polymer systems. For glassy networks, modes of dissipation are frozen out and unable to dissipate impact energy, while systems with lower T_g values have more molecular mobility under ambient conditions. In a homogeneous network, the ability or inability for polymer segments to move and dissipate energy is the difference between energy being dissipated and mechanical failure.

The GDMP-TATAT network demonstrated anomalous behavior compared with the other TENs (point B in Figure 6). For this particular network, the peak force was much lower. As mentioned above, this system is in a region, under ambient temperatures, whereby the tan δ in DMA is above 0.3. This result is similar to what was observed in pendulum impact results and is again attributable to additional modes of energy dissipation via viscoelastic dissipation in the vicinity of the glass transition temperature.

When compared to EVA (point A in Figure 6), TENs with similar T_g values all demonstrate lower peak force values, and thus potentially better impact performance for this test type. We believe that the higher peak force values of EVA material originate in its underlying network morphology. The crystalline domains of EVA are rigid with respect to its amorphous domain, and these physical cross-links prohibit motion.

Dependence of Peak Force on M_c and Monomer Rigidity. In these studies, we utilized two different alkene components in the network formation. It was found that networks from TATAT had higher T_g values compared with APE, but both networks had comparable cross-link densities in the rubber plateau region of the DMA. It might be expected that viscoelastic dissipation and energy management during an impact event may be related to the distance between elastically effective junction points within the network. For example, tighter networks have more junction points per unit volume (i.e., fewer linear chains between junction points that can dissipate energy between junction points.) Figure 7 shows the peak force from the impact experiments as a function of M_c for the TENs. On the basis of the resulting curve, we observe two behaviors: (1) systems synthesized with the more rigid TATAT monomer have higher peak forces in general, and (2) regardless of the alkene component, at some critical M_c the impact behavior becomes independent of M_c.

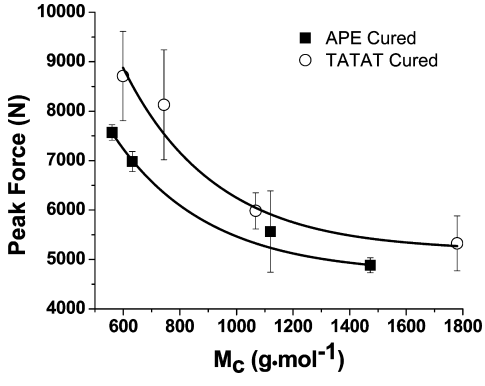

Figure 7. Peak force versus M_c for TENs. The line is a guide to the eye.

The first observation is likely due to polymer density, which is in turn related to the packing efficiency of the monomers. Upon the impact event, waves of energy propagate through the material, and if chain segments are mobile, this energy is absorbed by way of molecular motions. In contrast, more rigid systems would tend to restrict motions, decreasing damping processes. The second observation that a threshold exists whereby peak force becomes independent of M_c may be explained by a length scale phenomena. An applied force at the end of a chain will dissipate as it propagates down the chain. In a network, if the linear region between junction points is long enough (or the chains have enough mobility), the energy will dissipate completely before reaching the next junction point. Under this condition, the relaxation becomes effectively like a thermoplastic, and the number of elastically effective chains would vanish. We believe that the effect at high M_c is similar to this analogy; by increasing M_c, the elastic effects of the junction points within the networks become less evident and the T_g decreases (see Figure S4 in the Supporting Information) The extremely low peak force values associated with GDMP-TATAT could be explained by a synergistic effect of high M_c, high viscoelastic dissipation, and low T_g. It should also be noted that systems with high M_c might appear to be excellent choices for damping materials based on peak force, but the lack of mechanical robustness or structural integrity of many loosely cross-linked TENs in this region may not be sufficient for realistic applications without some improvement in toughness first.

Frequency Dependence and Damping Effects of TENs. It is well-known that the glass transition temperature is frequency dependent such that at higher frequency T_g shifts to higher values. In the case of using TENs as mouthguard materials, this could significantly affect damping properties at intraoral temperatures. If we know how the glass transition temperature shifts with increasing frequency, it would provide a better idea about the actual use conditions of the material. To study this effect, we considered the frequency dependence in tan δ_{max} for three TEN systems containing TATAT as the alkene component. If we assume the frequency dependence follows an Arrhenius relation, an effective activation energy can be extracted from a plot of ln f vs. reciprocal T_g.

$$\ln(f) = \ln(f_0) - \frac{E_a}{R}\frac{1}{T_g}$$

Figure 8 presents Arrhenius plots for three TATAT-based networks. The increase in T_g for these systems was about seven Kelvin per decade increase in frequency. The effective E_a of the glass transition was determined from the slope of the ln f vs. reciprocal T_g plot. ETTMP-TATAT and TMPT-TATAT showed effective E_a values around 300 kJ/mol, whereas GDMP-TATAT was around 220 kJ/mol. Note that the former two networks both have a higher total functionality compared with the GDMP-TATAT. Nonetheless, these are typical E_a values for the glass transition temperature.[6]

In addition, the dissipated heat (Q) can be determined from DMA analysis at one specific temperature utilizing stress (σ_o), strain (ε_o), and phase lag (δ) for one cycle.

$$Q = \pi\sigma_o\varepsilon_o \sin\delta$$

Note that the heat dissipation is solely dependent on the loss modulus (E'') through the in-phase component of phase lag (sin δ). Here we calculated heat dissipated at 38 °C (intraoral) temperature for TMPT-TATAT as a function of frequency. We

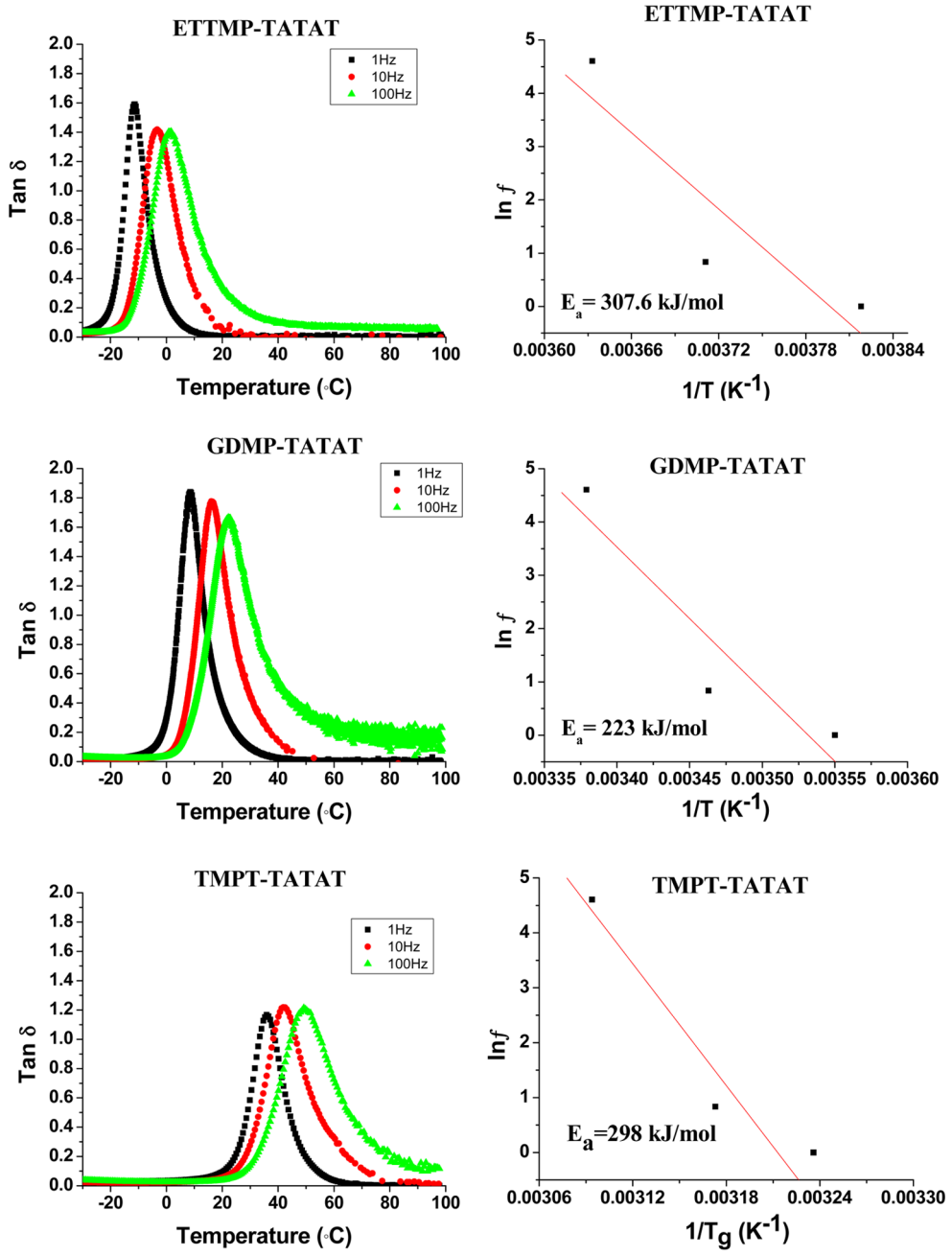

Figure 8. (left) Tan δ versus temperature for thiol−ene networks, ETTMP700-TATAT, GDMP-TATAT, and TMPT-TATAT at 0.1 (ETTMP700-TATATonly), 1, 10, and 100 Hz. (Right) Natural log of frequency versus tan δ max.

specifically chose this system due to the overlap of viscoelastic dissipation and the temperature of interest. Figure 9 shows E'' vs. temperature for TMPT-TATAT at four frequencies, 0.1, 1, 10, and 100 Hz, and the corresponding heat dissipation. We found there is a direct correlation between heat dissipated and frequency, i.e., as the frequency increases, E'' at 38 °C increases with a corresponding increase in Q. At much higher frequencies, the E'' peak would likely lie outside the range of 38 °C and damping would trend down to zero. This is a highly relevant tool for finding optimal conditions for a damping system.

CONCLUSIONS

In this study, we investigated the impact properties of unmodified thiol−ene networks with similar M_c values and differing monomer rigidity. We demonstrate a broad range of T_g values achievable via the UV photopolymerization of commercial thiol and alkene monomers. We correlated the effect of the rigid monomers with respect to T_g and impact properties. Most importantly, we were able to demonstrate the relationship between T_g and peak force of an impact event. The effects of junction points and impact performance were also explored and a critical length scale of energy dissipation was determined based on peak force values with respect to M_c. We determined that time to peak force was lower for higher T_g systems, whereas networks with T_g values comparable to EVA demonstrated much lower peak force values compared to EVA. The higher peak force values of EVA is likely an effect of the rigid crystalline domains of the semi-crystalline polymer which. Impact properties of TENs appear to be fairly predictable unless the testing temperature overlaps the temperature range wherein viscoelastic dissipation is

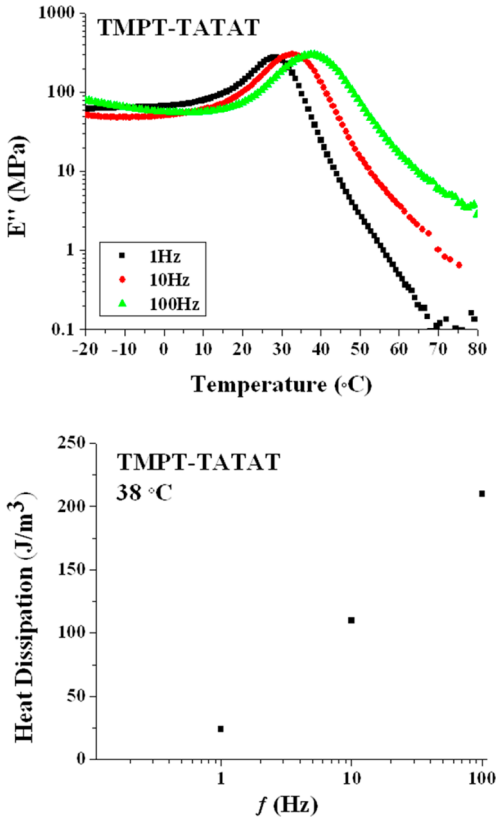

Figure 9. (Top) E'' vs temperature for TMPT-TATAT at 1, 10, and 100 Hz. (Bottom) Heat dissipation (Q) at 38 °C for TMPT-TATAT at 1, 10, and 100 Hz.

effective. Until now, a platform for impact properties for TENs has not been established. Research from this investigation can be utilized in future studies to determine specific systems for damping applications at various temperatures.

■ ASSOCIATED CONTENT

Ⓢ Supporting Information

Additional figures (PDF). This material is available free of charge via the Internet at http://pubs.acs.org.

■ AUTHOR INFORMATION

Corresponding Author

*E-mail: daniel.savin@usm.edu. Phone: 601-266-5395. Fax: 601-266-5504.

Notes

The authors declare no competing financial interest.

■ ACKNOWLEDGMENTS

The authors gratefully acknowledge funding from the Office of Naval Research (Award N00014-07-1-1057). O.D.M. was supported by the U.S. Department of Education GAANN Fellowship Program (Award P200A090066). A.P.J. was supported by a fellowship from the National Science Foundation GK-12 program "Connections in the Classroom: Molecules to Muscles", Award 0947944, through the University of Southern Mississippi. We thank Bruno Bock Thio-Chemicals-S for graciously donating thiol monomers.

■ REFERENCES

(1) Hartmann, B.; Lee, G. F.; Lee, J. D. *J. Acoust. Soc. Am.* **1994**, *95*, 226−233.
(2) Woo, L.; Westphal, S.; Ling, M. T. K. *Polym. Eng. Sci.* **1994**, *34*, 420−427.
(3) Heinrich, G.; Kluppel, M. In *Filled Elastomers Drug Delivery Systems*; Advances in Polymer Science; Springer: New York, 2002; Vol. *160*, pp 1−44.
(4) Rodriguez-Perez, M. A., Crosslinked polyolefin foams: Production, structure, properties, and applications. In *Crosslinking in Materials Science*; Ameduri, B., Ed.; Springer−Verlag: Berlin, 2005; Vol. *184*, pp 97−126.
(5) Knapik, J.; Marshall, S.; Lee, R.; Darakjy, S.; Jones, S.; Mitchener, T.; Cruz, G.; Jones, B. *Sports Med.* **2007**, *37*, 117−144.
(6) Menard, K. P., *Dynamic Mechanical Analysis: A Practical Introduction*, 2nd ed.; CRC Press: Boca Raton, FL, 2008; pp 123−144.
(7) Gould, T. E.; Piland, S. G.; Shin, J.; Hoyle, C. E.; Nazarenko, S. *Dent. Mater.* **2009**, *25*, 771−780.
(8) Westerman, B.; Stringfellow, P. M.; Eccleston, J. A. *Dent. Traumatol.* **2002**, *18*, 24−27.
(9) Newsome, P. R. H.; Tran, D. C.; Cooke, M. S. *Int. J. Paediatr. Dent.* **2001**, *11*, 396−404.
(10) Odian, G. *Principles of Polymerization*, 4th ed.; John Wiley and Sons: Hoboken, NJ, 2004; pp 530−531.
(11) Moly, K. A.; Bhagawan, S. S.; Groeninckx, G.; Thomas, S. *J. Appl. Polym. Sci.* **2006**, *100*, 4526−4538.
(12) Patrick, D. G.; van Noort, R.; Found, M. S. *Composites, Part A* **2006**, *37*, 1423−1427.
(13) Hoyle, C. E.; Lee, T. Y.; Roper, T. *J. Polym. Sci., Part A: Polym. Chem.* **2004**, *42*, 5301−5338.
(14) Senyurt, A. F.; Wei, H.; Phillips, B.; Cole, M.; Nazarenko, S.; Hoyle, C. E.; Piland, S. G.; Gould, T. E. *Macromolecules* **2006**, *39*, 6315−6317.
(15) Okay, O.; Reddy, S. K.; Bowman, C. N. *Macromolecules* **2005**, *38*, 4501−4511.
(16) Hoyle, C. E.; Lowe, A. B.; Bowman, C. N. *Chem. Soc. Rev.* **2010**, *39*, 1355−1387.
(17) Hoyle, C. E.; Bowman, C. N. *Angew. Chem., Int. Ed.* **2010**, *49*, 1540−1573.
(18) Wei, H. Y.; Senyurt, A. F.; Jonsson, S.; Hoyle, C. E. *J. Polym. Sci., Part A: Polym. Chem.* **2007**, *45*, 822−829.
(19) Senyurt, A. F.; Wei, H. Y.; Hoyle, C. E.; Piland, S. G.; Gould, T. E. *Macromolecules* **2007**, *40*, 4901−4909.
(20) Senyurt, A. F.; Hoyle, C. E.; Wei, H.; Piland, S. G.; Gould, T. E. *Macromolecules* **2007**, *40*, 3174−3182.
(21) *ASTM Standard D2240: Standard Test Method for Rubber Property—Durometer Hardness*; ASTM International: West Conshohocken, PA, 2005; DOI: 10.1520/D2240-05R10, www.astm.org.
(22) Heimenz, P. C., Lodge, T. P., *Polymer Chemistry*, 2nd ed.; CRC Press: Boca Raton, FL, 2007; pp 419−510.
(23) *ASTM Standard D6110: Standard Test Method for Determining the Charpy Impact Resistance of Notched Specimens of Plastics*; ASTM International, West Conshohocken, PA, 2006; DOI: 10.1520/D6110-10, www.astm.org.
(24) Krzeminski, D.; Goetz, J.; Janisse, A.; Lippa, N.; Gould, T.; Rawlins, J.; Piland, S. *Sports Technol.* **2011**, *4*, 65−76.
(25) Westerman, B.; Stringfellow, P. M.; Eccleston, J. A. *Br. J. Sports Med.* **2002**, *36*, 51−53.
(26) Li, Q.; Zhou, H.; Hoyle, C. E. *Polymer* **2009**, *50*, 2237−2245.
(27) Hoyle, C. E.; Gould, T.; Piland, S.; Wei, H.; Phillips, B.; Nazarenko, S.; Askim, F.; Cole, M. *Radtech Rep.* **2006**, 12−17.
(28) Kade, M. J.; Burke, D. J.; Hawker, C. J. *J. Polym. Sci., Part A: Polym. Chem.* **2010**, *48*, 743−750.
(29) McNair, O. D.; Sparks, B. J.; Janisse, A. P.; Brent, D. P.; Patton, D. L.; Savin, D. A. *Macromolecules* **2013**, *46*, 5614−5621.
(30) Li, Q.; Zhou, H.; Wicks, D. A.; Hoyle, C. E. *J. Polym. Sci., Part A: Polym. Chem.* **2007**, *45*, 5103−5111.